



# Many-body factorization and position-momentum equivalence of nuclear short-range correlations

R. Cruz-Torres<sup>1,10</sup>, D. Lonardoni<sup>1,2,3,10</sup>, R. Weiss<sup>4</sup>, M. Piarulli<sup>5</sup>, N. Barnea<sup>4</sup>, D. W. Higinbotham<sup>1,6</sup>, E. Piasetzky<sup>7</sup>, A. Schmidt<sup>1,6</sup>, L. B. Weinstein<sup>8</sup>, R. B. Wiringa<sup>9</sup> and O. Hen<sup>1,6</sup>✉

**While mean-field approximations, such as the nuclear shell model, provide a good description of many bulk nuclear properties, they fail to capture the important effects of nucleon-nucleon correlations such as the short-distance and high-momentum components of the nuclear many-body wave function<sup>1</sup>. Here, we study these components using the effective pair-based generalized contact formalism<sup>2,3</sup> and ab initio quantum Monte Carlo calculations of nuclei from deuteron to  $^{40}\text{Ca}$  (refs. <sup>4–6</sup>). We observe a universal factorization of the many-body nuclear wave function at short distance into a strongly interacting pair and a weakly interacting residual system. The residual system distribution is consistent with that of an uncorrelated system, showing that short-distance correlation effects are predominantly embedded in two-body correlations. Spin- and isospin-dependent ‘nuclear contact terms’ are extracted in both coordinate and momentum space for different realistic nuclear potentials. The contact coefficient ratio between two different nuclei shows very little dependence on the nuclear interaction model. These findings thus allow extending the application of mean-field approximations to short-range correlated pair formation by showing that the relative abundance of short-range pairs in the nucleus is a long-range (that is, mean field) quantity that is insensitive to the short-distance nature of the nuclear force.**

Short-range correlations (SRCs) emerge from pairs of nucleons having large relative momentum compared to their centre-of-mass (c.m.) momentum and to the typical nuclear Fermi momentum  $k_F \approx 250 \text{ MeV}/c$  (ref. <sup>1</sup>). At momenta just above  $k_F$  ( $300 \leq k \leq 600 \text{ MeV}/c$ ), they are primarily due to proton-neutron (*pn*) pairs and are thought to dominate the nuclear wave function<sup>1,7–10</sup>. At larger momentum, the fraction of proton-proton (*pp*) pairs increases, possibly due to their sensitivity to the repulsive core of the nuclear interaction<sup>11,12</sup>. SRCs have substantial implications for the internal structure of nucleons bound in nuclei<sup>1,13,14</sup>, neutrinoless double beta decay matrix elements<sup>15,16</sup>, nuclear charge radii<sup>17</sup> and neutron star properties<sup>18</sup>. Therefore, understanding their formation mechanisms and specific characteristics is required for obtaining a complete description of atomic nuclei.

As nucleons in short-range correlated pairs have substantial spatial overlap and are far off their mass shell ( $E^2 - p^2 < m^2$ , where  $E$  is the nucleon energy,  $p$  is its momentum and  $m$  is the free nucleon mass), their theoretical description poses a major challenge. Ab initio many-body calculations using different interaction models pro-

duce wave functions that substantially differ at short distances and high momenta<sup>4,19</sup> (Extended Data Fig. 1). This is generally referred to as ‘scale and scheme dependence’, where ‘scheme’ refers to the type of interaction (for example, phenomenological or derived from chiral effective field theory,  $\chi$ EFT), and ‘scale’ refers to the regulation cut-off inherent to EFT models. This dependence raises important questions about the model dependence of the interpretation of SRC measurements and of their implications.

To address this, we employ the pair-based generalized contact formalism (GCF)<sup>3,3</sup> to study the scale and scheme dependence of different SRC properties, as extracted from many-body ab initio quantum Monte Carlo (QMC) calculations of nuclei with nucleon number  $A$  from  $A = 2$  to  $40$  (refs. <sup>4–6,19–21</sup>) performed using different realistic nuclear interaction models.

The GCF exploits the scale separation between the strong interaction among the nucleons in a short-range correlated pair and the pair’s weaker interaction with its surroundings<sup>2,3,22</sup>. Using this scale separation, the two-nucleon density in either coordinate or momentum space (that is, probability of finding two nucleons with relative and c.m. momenta  $q$  and  $Q$ , respectively, or with separation  $r$  and distance  $R$  from the nucleus c.m.<sup>4</sup>) can be expressed at small separation or high relative momentum as<sup>3</sup>:

$$\begin{aligned} \rho_{\alpha,NN}^A(R, r) &= C_{\alpha,NN}^A(R) \times |\varphi_{NN}^\alpha(r)|^2, \\ n_{\alpha,NN}^A(Q, q) &= \tilde{C}_{\alpha,NN}^A(Q) \times |\tilde{\varphi}_{NN}^\alpha(q)|^2, \end{aligned} \quad (1)$$

where  $A$  denotes the nucleus,  $NN$  the nucleon pair (*pn*, *pp*, *nn*) and  $\alpha$  stands for the quantum state (spin 0 or 1).  $\varphi_{NN}^\alpha$  are universal two-body wave functions, given by the zero-energy solution of the two-body Schrödinger equation, and  $\tilde{\varphi}_{NN}^\alpha$  are their Fourier transforms (Extended Data Fig. 2).  $\varphi_{NN}^\alpha$  are universal in the weak sense, that is, they are nucleus independent but not model independent. Nucleus-dependent ‘nuclear contact coefficients’ are given by

$$\begin{aligned} C_{\alpha,NN}^A &\equiv \int dR C_{\alpha,NN}^A(R), \\ \tilde{C}_{\alpha,NN}^A &\equiv \frac{1}{(2\pi)^3} \int dQ \tilde{C}_{\alpha,NN}^A(Q), \end{aligned} \quad (2)$$

and define the number of  $NN$  SRC pairs in nucleus  $A$ .

The GCF construction relates short-distance and high-momentum physics such that  $C_{\alpha,NN}^A = \tilde{C}_{\alpha,NN}^A$ . Previous studies<sup>3</sup> showed the validity of this equality using QMC calculations of

<sup>1</sup>Massachusetts Institute of Technology, Cambridge, MA, USA. <sup>2</sup>Facility for Rare Isotope Beams, Michigan State University, East Lansing, MI, USA.

<sup>3</sup>Theoretical Division, Los Alamos National Laboratory, Los Alamos, NM, USA. <sup>4</sup>Racah Institute of Physics, The Hebrew University, Jerusalem, Israel.

<sup>5</sup>Physics Department, Washington University, St Louis, MO, USA. <sup>6</sup>Thomas Jefferson National Accelerator Facility, Newport News, VA, USA. <sup>7</sup>School of Physics and Astronomy, Tel Aviv University, Tel Aviv, Israel. <sup>8</sup>Old Dominion University, Norfolk, VA, USA. <sup>9</sup>Physics Division, Argonne National Laboratory, Lemont, IL, USA. <sup>10</sup>These authors contributed equally: R. Cruz-Torres, D. Lonardoni. ✉e-mail: hen@mit.edu

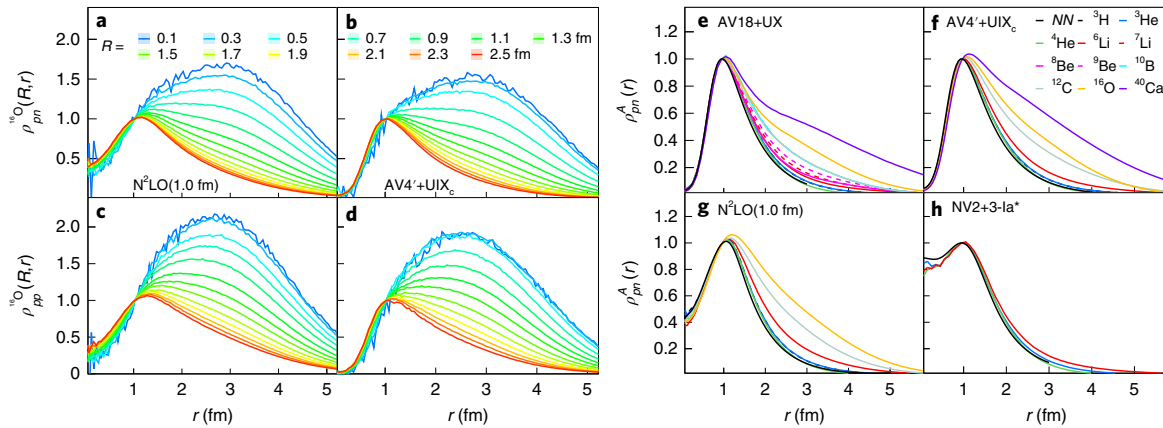


**Fig. 1 | Short-distance universality of two-nucleon density in nuclei.** QMC two-nucleon coordinate-space densities calculated using different NN+3N potentials. **a–d**,  $^{16}\text{O}$  relative-distance  $r$  densities  $\rho_{NN}^{16\text{O}}(R, r)$  for different pair centre-of-mass position  $R$  in the nucleus. Distributions are shown for  $pn$  (**a**, **b**) and  $pp$  (**c**, **d**) pairs and different interactions: AV4'+UIX<sub>c</sub> (**b**, **d**) and N<sup>2</sup>LO(1.0 fm) (**a**, **c**). **e–h**, Relative-distance  $pn$  pairs densities  $\rho_{pn}^A(r)$  for several nuclei (coloured lines) integrated over  $R$  and compared with the two-body universal function  $|\varphi_{pn}^{s=1}|^2$  (black lines). Distributions are shown for both the phenomenological AV18+UX (**e**) and AV4'+UIX<sub>c</sub> (**f**) and the chiral N<sup>2</sup>LO(1.0 fm) (**g**) and NV2+3-Ia\* (**h**) interactions. For each interaction, all calculations are scaled to have the same value at  $\sim 1$  fm, thus highlighting their same short-distance behaviour for all nuclei. The difference between  $NN$  distributions in the same nucleus obtained using different interactions, as shown by the four panels, indicates the scale and scheme dependence of the many-body calculations. Equivalent  $pp$  distributions are presented in Extended Data Fig. 4.

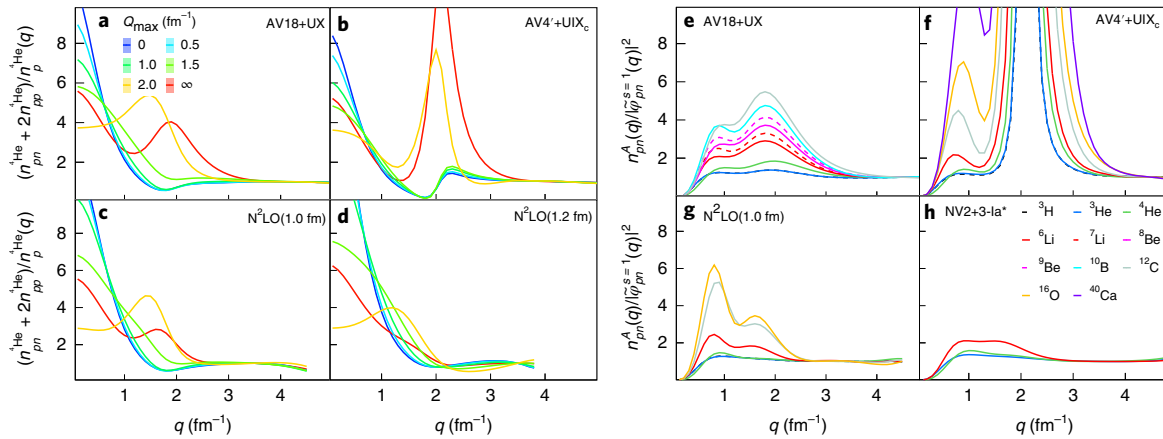


**Fig. 2 | High-momentum universality of two-nucleon density in nuclei.** QMC two-nucleon momentum-space distributions calculated using different phenomenological (AV18+UX and AV4'+UIX<sub>c</sub>) and chiral (N<sup>2</sup>LO(1.0 fm), N<sup>2</sup>LO(1.2 fm) and NV2+3-Ia\*) potentials. All the curves are normalized to unity at high momentum (4.5 fm<sup>-1</sup> and 3.5 fm<sup>-1</sup> for phenomenological and chiral interactions, respectively). **a–d**,  $^4\text{He}$  pair relative-momentum  $q$  distributions  $n_{NN}^A(Q, q)$  integrated over pair centre-of-mass momentum  $Q$  between 0 and  $Q_{\max}$  and divided by the one-body momentum distribution. Scaling onset is observed close to  $q \approx k_F$  (the nuclear Fermi momentum) for  $Q_{\max}$  between 0 and  $k_F$  and is pushed to higher  $q$  values with increasing  $Q_{\max}$ . **e–h**, Two-nucleon relative-momentum distribution ratios,  $n_{pn}^A(q)/|\tilde{\varphi}_{pn}^{s=1}(q)|^2$ , integrated over  $Q$ . Scaling is clearly observed at high momenta, starting at 3.5–4 fm<sup>-1</sup> for the phenomenological potentials (**e**, **f**), and at 2–2.5 fm<sup>-1</sup> for the chiral interactions (**g**, **h**). The N<sup>2</sup>LO 1.0 fm and 1.2 fm distributions are only shown up to 4.4 and 3.8 fm<sup>-1</sup>, respectively, above which statistics is poor and regulator/cut-off artefacts dominate. Equivalent  $pp$  distributions are presented in Extended Data Fig. 4.

$\rho_{\alpha,NN}^A(r) \equiv \int dR \rho_{\alpha,NN}^A(R, r)$  and  $n_{\alpha,NN}^A(q) \equiv \int dQ n_{\alpha,NN}^A(Q, q)$  for  $A = 2$  to 40 using the AV18+UX interaction<sup>23</sup>. More recently, refs. <sup>21,24</sup> analysed QMC calculations of  $\rho_{\alpha,NN}^A(r)/\rho_{\alpha,NN}^d(r)$  ratios obtained using three additional interactions (without separating different spin-isospin channels), showing first evidence for short distances scale-and-scheme independence.

Here we study the applicability of the GCF for modelling nuclear systems using new QMC calculations of  $\rho_{\alpha,NN}^A(r, R)$  and  $n_{\alpha,NN}^A(q, Q)$ , projected into spin-isospin channels, for different nuclei and  $NN$  potentials (AV18+UX, AV4'+UIX<sub>c</sub>, N<sup>2</sup>LO(1.0 fm), N<sup>2</sup>LO(1.2 fm), and NV2+3-Ia\*). See Extended Data Fig. 3 and Methods for details.

Figure 1a–d shows the relative-distance densities of  $np$  and  $pp$  pairs in oxygen  $\rho_{NN}^{16\text{O}}(R, r)$  for different values of  $R$  and for two different interactions: AV4'+UIX<sub>c</sub> and N<sup>2</sup>LO(1.0 fm). All densities were scaled to the same value at  $r = 1$  fm. This highlights the similarities of the different distributions at  $r \leq 1$  for all values of  $R$ , showcasing the existence of short-distance factorization.

Calculations of  $\rho_{\alpha,NN}^A(r, R)$  are computationally demanding and are not available for all nuclei and interactions. We thus explore the nucleus and interaction independence of the short-distance factorization using  $\rho_{\alpha,NN}^A(r) = \int dR \rho_{\alpha,NN}^A(R, r)$  calculations. Figure 1e–h shows the  $pn$ -pair densities  $\rho_{pn}^A(r)$  for four interactions and different nuclei. While the short-distance behaviour of  $\rho_{pn}^A(r)$  is different

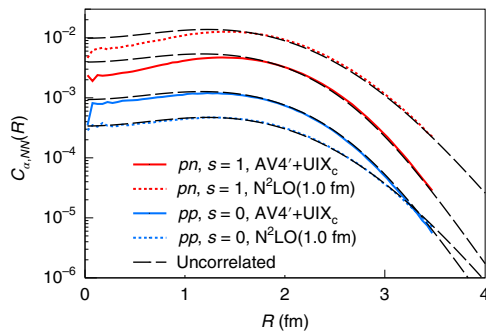


**Fig. 3 | Nuclear contact density distribution.** Absolute contact distributions  $C_{\alpha,NN}^{16O}(R)$  obtained from QMC two-nucleon coordinate-space densities integrated over  $r$  from 0 to 1 fm. Distributions are shown for  $pn$  (red) and  $pp$  (blue) pairs, calculated using the phenomenological AV4'+UIX<sub>c</sub> (solid lines) and chiral N<sup>2</sup>LO(1.0 fm) (dotted lines) interactions. The dashed black curves correspond to extraction using uncorrelated densities obtained using a convolution of the single-nucleon density distribution with itself. The uncorrelated distributions are scaled by 0.87 ( $pp$ ) and 0.65 ( $pn$ ) to match the magnitude of the QMC distributions. See text for details.

for each interaction, it is the same for all nuclei, and can thus be described by the GCF's two-body universal functions. This validates the factorization of equation (1) in position space.

The equivalent study of two-nucleon momentum distributions  $n_{NN}^A(q)$  is more delicate.  $n_{NN}^A(Q, q)$  include combinatorial contributions from all possible pairs of nucleons, not just nucleon pairs in SRC states. Two nucleons each belonging to a different SRC pair have high individual momenta that can add to give both high relative and high c.m. momenta. In coordinate-space calculations these non-SRC pairs are suppressed by requiring small pair separation. In momentum space, excluding such pairs requires either low c.m. momenta or much higher relative momenta<sup>3</sup>.

This can be seen by examining the  $q$  dependence of the ratio of the integrated two-body density to the one-body density in  ${}^4He$ ,  $[\int_0^{Q_{\max}} (n_{np}^{4He}(Q, q) + 2n_{pp}^{4He}(Q, q)) dQ]/n_p^{4He}(q)$ , for different values of  $Q_{\max}$  (Fig. 2a-d). Here  $n_p^{4He}(q)$  is the probability density of finding a proton in the nucleus with momentum  $q$ . The ratio should scale (be constant with  $q$ ) when both the one- and two-body densities are dominated by the same correlated SRC pairs. As can be seen, the ratio scales for high  $q$  with a scaling onset that seems to go down as  $Q_{\max}$  is lowered from infinity to values between zero and  $k_F$  (the characteristic c.m. momentum scale of SRC pairs<sup>3,22</sup>). This is caused by the inclusion of uncorrelated pairs that push the scaling to higher  $q$  when integrating over very high  $Q_{\max}$  values.

Figure 2e-h shows the  $n_{pn}^A(q)/|\vec{q}_{pn}^{s=1}(q)|^2$  ratio for a variety of nuclei and interactions. As expected from equation (1), these ratios scale (that is, are constant) at high momenta. For  $pn$  pairs the scaling is clear. For  $pp$  pairs (Extended Data Fig. 4) it is less pronounced, but it is still visible starting at slightly higher momenta than the equivalent  $pn$  scaling.

Having established the GCF factorization of equation (1), we turn to examine the nuclear contact terms  $C_{\alpha,NN}^A$ . These encapsulate the many-body dynamics driving the formation of SRC pairs. They should be scale separated from the correlated two-body part and thus be less sensitive to the short-distance  $NN$  interaction.

Figure 3 shows  $C_{\alpha,NN}^{16O}(R)$  for  $np$  and  $pp$  SRC pairs in oxygen, obtained using equation (1). The QMC contact distributions are in good agreement with calculations of uncorrelated pairs obtained from single-nucleon density distributions (see Methods for details). This agreement is insensitive to the pair separation integration limit

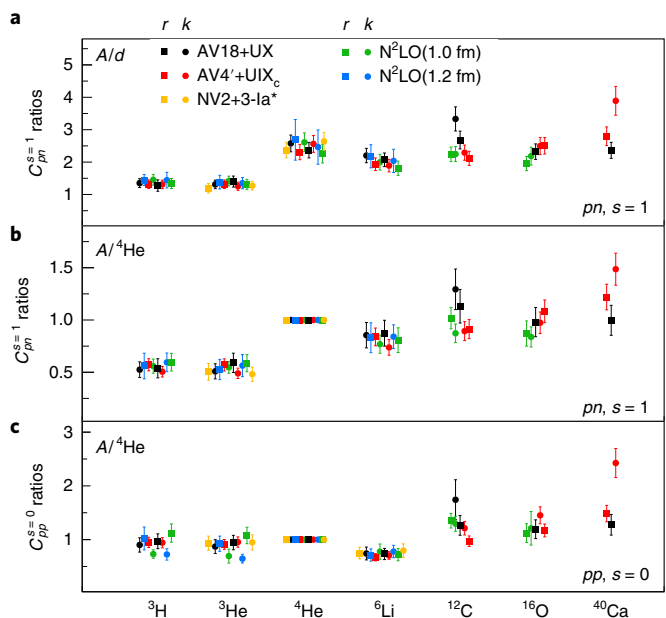


**Fig. 4 | Spin-dependent nuclear contact term ratios.** **a–c,** Ratios of spin-1  $pn$  contact terms ( $C_{pn}^{s=1}$ ) for different nuclei to deuteron (a) or  ${}^4He$  (b), and of spin-0  $pp$  contact terms ( $C_{pp}^{s=0}$ ) for different nuclei to  ${}^4He$  (c). The contact terms ratios were extracted using different  $NN+3N$  potentials in both coordinate ( $r$ , squares) and momentum ( $k$ , circles) space. The contact values for  ${}^3H$  for spin-0  $pp$  in c correspond to  $C_{pn}^{s=0}({}^3H)$ , as there are no  $pp$  pairs in this nucleus. All the contacts  $C_{\alpha,NN}^A(A)$  are divided by  $A/2$  and multiplied by 100. Error bars show the combined statistical and extraction systematical uncertainties at the  $1\sigma$  or 68% confidence level.

from 0 to 1 fm. This shows that the density distribution of SRC pairs (that is, shape of  $C_{\alpha,NN}^{16O}(R)$ ) only depends on the nuclear mean field, with minimal sensitivity to the short-distance  $NN$  interaction.

To further corroborate this finding and its relevance for other nuclei, we examine the ratio of two-nucleon distributions in nucleus  $A$  relative to a reference nucleus  $A_0$ , that is,  $\rho_{\alpha,NN}^A(r)/\rho_{\alpha,NN}^{A_0}(r)$  and  $n_{\alpha,NN}^A(q)/n_{\alpha,NN}^{A_0}(q)$ . According to equation (1), for small  $r$  (large  $q$ ) these ratios should be independent of  $r(q)$  and equal to  $C_{\alpha,NN}^A/C_{\alpha,NN}^{A_0}$  ( $\tilde{C}_{\alpha,NN}^A/\tilde{C}_{\alpha,NN}^{A_0}$ ). They thus allow studying the  $A$ -dependence of the contacts, independent from the universal functions.

Figure 4 shows  $C_{s=1,pn}^A/C_{s=1,pn}^d$  and  $C_{\alpha,NN}^A/C_{\alpha,NN}^{{}^4He}$  (where  $s$  is the  $NN$  pair spin) for all available nuclei and interactions. The contact ratios for a given nucleus are consistent within uncertainties, that is, are largely scale- and scheme-independent. They are also the same for both short-distance and high-momentum pairs. The fact that models with very different short-range physics, including the tensorless AV4', all lead to the same contact term ratios supports our conclusion that these ratios are determined by mean-field physics (that is, by the average field of the other  $A - 2$  nucleons) and are insensitive to the details of the  $NN$  interaction at short distance.

This insensitivity can simplify calculations of heavier nuclei, which are very difficult with ‘hard’ interactions such as AV18. The contact term  $C_{\alpha,NN}^{A_0}$  can be calculated for  $d$  or  ${}^4He$  using the ‘hard’ interaction. It can then be extrapolated to heavier nuclei by multiplying by the appropriate contact term ratio  $C_{\alpha,NN}^A/C_{\alpha,NN}^{A_0}$  (where  $A_0 = d$  or  ${}^4He$ ) calculated using ‘soft’ interactions that are easier to compute.

Experimentally, measured inclusive ( $e, e'$ ) scattering cross-section ratios at large momentum transfer ( $Q^2 > 1.5 \text{ GeV}^2$ ) for nucleus with nucleon number  $A$  relative to the deuteron are used to determine

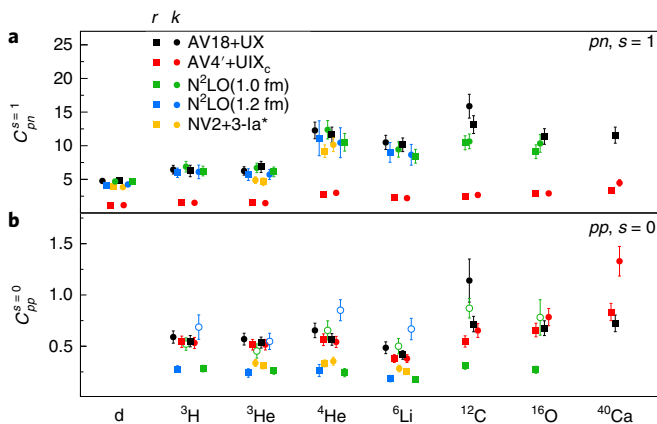


**Fig. 5 | Nuclear contact terms.** **a,b,** The absolute values of the spin-1  $pn$  (**a**) and spin-0  $pp$  (**b**) contact terms,  $C_{pn}^{s=1}$  and  $C_{pp}^{s=0}$ , respectively, for different nuclei extracted from QMC calculations in both coordinate ( $r$ , squares) and momentum ( $k$ , circles) space using different  $NN+3N$  potentials. The contact values for  ${}^3\text{H}$  for spin-0  $pp$  in **b** corresponds to  $C_{nn}^{s=0}({}^3\text{H})$ , as there are no  $pp$  pairs in this nucleus.  $k$ -space  $N^2\text{LO}$  spin-0  $pp$  contacts are marked with open symbols to highlight the difficulty in their extraction. See text for details. All the contacts  $C_{NN}^\alpha(A)$  are divided by  $A/2$  and multiplied by 100. Error bars show the combined statistical and extraction systematical uncertainties at the  $1\sigma$  or 68% confidence level.

an SRC scaling coefficient  $a_2(A/d)$ . This coefficient is traditionally interpreted as the relative abundance of SRC pairs in the measured nuclei<sup>25</sup>. In addition, it is claimed that comparisons of  $a_2(A/d)$  measurements over a range of symmetric and asymmetric nuclei are sensitive to the nature of the nuclear interaction.

Theoretically, refs. <sup>21,24</sup> showed that the relative abundance of short-distance  $NN$  pairs in nucleus  $A$  relative to the deuteron (that is,  $\rho^A(r)/\rho^d(r)$  for  $r \rightarrow 0$ , where  $\rho^A(r)$  includes all  $NN$  pairs) is insensitive to the choice of nuclear interaction, and is consistent with the measured  $a_2(A/d)$  for all nuclei considered. This raised doubts about the sensitivity of  $a_2(A/d)$  to the nuclear interaction. However, the connection between the measured  $a_2(A/d)$  and the calculated pair-distance distributions needs to be justified, as the universal function of equation (1) does not automatically cancel in the  $A/d$  ratio when all SRC channels are included<sup>26</sup>. Our observation that the calculated contact ratios are independent of the nuclear interaction in both coordinate and momentum space and for each pair quantum state separately bolsters and extends these observations.

Exclusive measurements of two-nucleon knockout  $A(e,e'NN)$  (refs. <sup>7–12</sup>) on the other hand are sensitive to the nuclear interaction model<sup>11,12</sup> (Extended Data Fig. 5). The GCF factorization, and the contact terms we extract, are key for relating measurements of nucleon knockout to different nuclear interaction models and ab initio many-body calculations<sup>11,27,28</sup>.

Reference <sup>29</sup> recently claimed a difference between the scaling of SRC pairs with high relative momenta, dominated by  $pn$  pairs, and pairs with small separation, having a combinatorial enhancement of  $pp$  pairs. This distinction questions the relation between SRC pairs and the modification of the internal structure of nucleons bound in nuclei, extractions of the free neutron structure from nuclear deep inelastic scattering measurements, and the determination of spin-flavour symmetry-breaking mechanisms in quantum chromodynamics (QCD)<sup>14</sup>. Our observation that both coordinate- and momentum-space contacts exhibit the same scaling show that the speculations of ref. <sup>29</sup> are inconsistent with QMC wave functions<sup>30</sup>.

Finally we examine the individual contacts. Figure 5 and Extended Data Fig. 6 show the contacts extracted by fitting

equation (1) to the individual two-nucleon QMC densities for different nuclei in either coordinate or momentum space. As can be seen, the extracted spin-1  $pn$  contacts are scale- and scheme-independent (that is, the same) for all interactions examined here, except for the AV4'+UIX<sub>c</sub>, as expected given its lack of a tensor force.

For spin-0  $pp$  contacts our results are more complex. The contacts extracted for phenomenological potentials agree with each other but are higher than those extracted for chiral potentials. This is understood to result from the cutoffs employed in chiral interactions, which have a larger impact on the spin-0  $pp$  channel due to the lack of a tensor force that otherwise would fill the minimum in the momentum distribution around  $2 \text{ fm}^{-1}$  (Extended Data Fig. 2).

Furthermore, the  $k$ -space  $N^2\text{LO}$  contacts disagree with their equivalent in  $r$ -space. As the NV2+3-Ia\* contacts do not show such a discrepancy, this issue is specific to the  $N^2\text{LO}$  potentials and is not an inherent feature of chiral potentials.

Examining the  $pp$  two-body universal functions, we see that they are very similar for NV2+3-Ia\* and  $N^2\text{LO}(1.0 \text{ fm})$  (Extended Data Fig. 2). In contrast, the  ${}^4\text{He}$   $pp$  momentum distributions differ at high momenta for the two potentials. This is most likely due to the combined effect of their different regulators, lower order in the chiral expansion, and lack of intermediate deltas in the  $N^2\text{LO}$  potential that enhances three-body effects that are absent in the GCF formulation of equation (1).

These regulator and three-body effects make it difficult to identify a clear high-momentum scaling plateau in the spin-0  $pp$  channel for  $N^2\text{LO}$  potentials. See Methods for details.

Indeed, when three-body forces and correlations are excluded from the calculation the  $k$ - and  $r$ -space  $N^2\text{LO}$  contacts are the same (Extended Data Fig. 7). Furthermore, the fact that the contact ratios of nucleus  $A$  to  ${}^4\text{He}$  are the same in  $r$ - and  $k$ -space for all channels and interactions (including for  $N^2\text{LO} pp$  pairs) implies that the effect leading to the  $N^2\text{LO} ppr-k$  discrepancy cancels in the ratio, and therefore does not extend beyond the three-body level. We thus can conclude that (1) the many-body ( $A \geq 3$ ) nuclear dynamics of the contact coefficients is the same for both coordinate and momentum space and is independent of the details of the  $NN$  interaction model, and (2) that any corrections that are missing in equation (1), and cause the  $N^2\text{LO}$  discrepancy, do not involve terms that go beyond the three-body level, which is why they cancel in the ratios of heavy nuclei to light ones.

## Online content

Any methods, additional references, Nature Research reporting summaries, source data, extended data, supplementary information, acknowledgements, peer review information; details of author contributions and competing interests; and statements of data and code availability are available at <https://doi.org/10.1038/s41567-020-01053-7>.

Received: 15 September 2019; Accepted: 2 September 2020;  
Published online: 9 November 2020

## References

- Hen, O., Miller, G. A., Piasetzky, E. & Weinstein, L. B. Nucleon-nucleon correlations, short-lived excitations, and the quarks within. *Rev. Mod. Phys.* **89**, 045002 (2017).
- Weiss, R., Bazak, B. & Barnea, N. Generalized nuclear contacts and momentum distributions. *Phys. Rev. C* **92**, 054311 (2015).
- Weiss, R., Cruz-Torres, R., Barnea, N., Piasetzky, E. & Hen, O. The nuclear contacts and short range correlations in nuclei. *Phys. Lett. B* **780**, 211–215 (2018).
- Wiringa, R. B., Schiavilla, R., Pieper, S. C. & Carlson, J. Nucleon and nucleon-pair momentum distributions in  $A \leq 12$  nuclei. *Phys. Rev. C* **89**, 024305 (2014).
- Lonardoni, D., Lovato, A., Pieper, S. C. & Wiringa, R. B. Variational calculation of the ground state of closed-shell nuclei up to  $A = 40$ . *Phys. Rev. C* **96**, 024326 (2017).

6. Lonardoni, D. et al. Properties of nuclei up to  $A = 16$  using local chiral interactions. *Phys. Rev. Lett.* **120**, 122502 (2018).
7. Subedi, R. et al. Probing cold dense nuclear matter. *Science* **320**, 1476–1478 (2008).
8. Korover, I. et al. Probing the repulsive core of the nucleon-nucleon interaction via the  ${}^4\text{He}(e,e'pN)$  triple-coincidence reaction. *Phys. Rev. Lett.* **113**, 022501 (2014).
9. Hen, O. et al. Momentum sharing in imbalanced Fermi systems. *Science* **346**, 614–617 (2014).
10. Duer, M. et al. Probing high-momentum protons and neutrons in neutron-rich nuclei. *Nature* **560**, 617–621 (2018).
11. Schmidt, A. et al. Probing the core of the strong nuclear interaction. *Nature* **578**, 540–544 (2020).
12. Korover, I. et al. Tensor-to-scalar transition in the nucleon-nucleon interaction mapped by  ${}^{12}\text{C}(e,e'pn)$  measurements. Preprint at <https://arxiv.org/abs/2004.07304> (2020).
13. Schmookler, B. et al. Modified structure of protons and neutrons in correlated pairs. *Nature* **566**, 354–358 (2019).
14. Segarra, E. P. et al. Neutron valence structure from nuclear deep inelastic scattering. *Phys. Rev. Lett.* **124**, 092002 (2020).
15. Simkovic, F., Faessler, A., Muther, H., Rodin, V. & Stauf, M. The  $0\nu\beta\beta$ -decay nuclear matrix elements with self-consistent short-range correlations. *Phys. Rev. C* **79**, 055501 (2009).
16. Cirigliano, V. et al. New leading contribution to neutrinoless double- $\beta$  decay. *Phys. Rev. Lett.* **120**, 202001 (2018).
17. Miller, G. A. et al. Can long-range nuclear properties be influenced by short range interactions? A chiral dynamics estimate. *Phys. Lett. B* **793**, 360–364 (2019).
18. Li, B. A., Cai, B.-J., Chen, L. W. & Xu, J. Nucleon effective masses in neutron-rich matter. *Prog. Part. Nucl. Phys.* **99**, 29–119 (2018).
19. Lonardoni, D., Gandolfi, S., Wang, X. B. & Carlson, J. Single- and two-nucleon momentum distributions for local chiral interactions. *Phys. Rev. C* **98**, 014322 (2018).
20. Lonardoni, D. et al. Auxiliary field diffusion Monte Carlo calculations of light and medium-mass nuclei with local chiral interactions. *Phys. Rev. C* **97**, 044318 (2018).
21. Lynn, J. et al. Ab initio short-range-correlation scaling factors from light to medium-mass nuclei. *J. Phys. G* **47**, 045109 (2020).
22. Cohen, E. O. et al. Center of mass motion of short-range correlated nucleon pairs studied via the  $A(e,e'pp)$  reaction. *Phys. Rev. Lett.* **121**, 092501 (2018).
23. Wiringa, R. B., Stoks, V. G. J. & Schiavilla, R. Accurate nucleon-nucleon potential with charge-independence breaking. *Phys. Rev. C* **51**, 38–51 (1995).
24. Chen, J. W., Detmold, W., Lynn, J. E. & Schwenk, A. Short range correlations and the EMC effect in effective field theory. *Phys. Rev. Lett.* **119**, 262502 (2017).
25. Egriyan, K. S. et al. Observation of nuclear scaling in the  $A(e,e')$  reaction at  $x_B \geq 1$ . *Phys. Rev. C* **68**, 014313 (2003).
26. Weiss, R. et al. Study of inclusive electron scattering scaling using the generalized contact formalism. Preprint at <https://arxiv.org/abs/2005.01621> (2020).
27. Weiss, R., Korover, I., Pisetsky, E., Hen, O. & Barnea, N. Energy and momentum dependence of nuclear short-range correlations—spectral function, exclusive scattering experiments and the contact formalism. *Phys. Lett. B* **791**, 242–248 (2019).
28. Pybus, J. R. et al. Generalized contact formalism analysis of the  ${}^4\text{He}(e,e'pN)$  reaction. *Phys. Lett. B* **805**, 135429 (2020).
29. Arrington, J. & Fomin, N. Searching for flavor dependence in nuclear quark behavior. *Phys. Rev. Lett.* **123**, 042501 (2019).
30. Hen, O. et al. Comment on ‘Searching for flavor dependence in nuclear quark behavior’. Preprint at <https://arxiv.org/abs/1905.02172> (2019).

**Publisher's note** Springer Nature remains neutral with regard to jurisdictional claims in published maps and institutional affiliations.

© The Author(s), under exclusive licence to Springer Nature Limited 2020

## Methods

**Universal function normalization.** While the normalizations of two-nucleon densities are well defined by the total number of nucleons in the nucleus, the individual normalizations of  $C_{\alpha,NN}^A$  and  $|\varphi_{NN}^\alpha(q)|^2$  are not. We therefore chose to normalize  $|\varphi_{NN}^\alpha(q)|^2$  such that its integral above  $q_s = 1.3 \text{ fm}^{-1}$  ( $\approx k_F$ ) equals unity<sup>3</sup>,  $\int_{q_s} \frac{4\pi}{(2\pi)^3} q^2 dq |\varphi_{NN}^\alpha(q)|^2 = 1$ . This defines the normalization of  $\varphi_{NN}^\alpha(r)$  via a Fourier transform and that of  $C_{\alpha,NN}^A$  and  $\tilde{C}_{\alpha,NN}^A$  via equation (1).

**Nucleon–nucleon interaction models.** The phenomenological AV18 (ref. <sup>23</sup>) and AV4' (ref. <sup>31</sup>) potentials are ‘hard interactions’, with a notable probability for nucleons to have high momentum ( $k > 3 \text{ fm}^{-1} \approx 600 \text{ MeV}/c$ ). Their derivation is similar, with AV4' being a reprojection of AV18 into four spin-isospin channels, not including the tensor interaction. Both potentials are supported by 3N forces that provide a good description of all nuclei considered in this work<sup>5,21</sup>.

The N<sup>3</sup>LO (refs. <sup>20,32,33</sup>) and NV2+3-1a\* (refs. <sup>34–36</sup>) interactions are fundamentally different, as they are based on a chiral perturbation expansion. The short-distance regulators used in these potentials make them softer, that is, their single-nucleon momentum distributions have less high-momentum strength as compared with AV18 and AV4' (Extended Data Figs. 1 and 2). The N<sup>3</sup>LO interactions include operators up to third order in the chiral expansion. The NV2+3-1a\* interaction considers nucleons plus explicit intermediate deltas, and includes all terms up to third order plus leading order N<sup>3</sup>LO terms.

All NN potentials used in this work have accompanying 3N potentials (three-body forces or 3BF) optimized to properly describe properties of light nuclei, such as binding energies,  $n$ - $\alpha$  scattering and  $\beta$ -decay rates.

**QMC calculations.** The QMC calculations used in this work include both variational Monte Carlo (VMC) and diffusion Monte Carlo (DMC) techniques. For each potential, a fully correlated many-body wave function is constructed and optimized in order to minimize the variational energy expectation value. Such a trial wave function is then propagated in imaginary time via DMC techniques, in order to project it onto the true ground state of the system and, therefore, to gain access to ground-state properties. Many physical quantities, such as two-nucleon distributions, can be extracted from both VMC and DMC calculations<sup>20</sup>. However, momentum-space calculations are currently available only from VMC calculations<sup>4,19</sup>, therefore for consistency we only present VMC results. At short distance, VMC coordinate-space distributions are almost identical to the DMC results. We use the differences as a measure of the QMC uncertainty (Extended Data Fig. 8).

**Uncorrelated two-nucleon density calculations.** Uncorrelated two-nucleon densities are given by a convolution of the single-nucleon density distribution,  $\rho_N^{16\text{O}}(R)$ , with itself,  $C_{NN,\text{uncorr.}}^{16\text{O}}(R) \equiv \int_0^{1\text{fm}} d\Omega_R dr \rho_N^{16\text{O}}(\mathbf{R} + \mathbf{r}/2) \rho_N^{16\text{O}}(\mathbf{R} - \mathbf{r}/2)$ , accounting for the Pauli exclusion principle for  $pp$  pairs, following ref. <sup>37</sup>. The two-body density is normalized to the number of nucleon pairs in the nucleus.

**Nuclear contact extraction.** The nuclear contact terms were extracted independently for both coordinate and momentum space by fitting the universal two-body wave functions in coordinate and momentum space to the corresponding two-body coordinate density or momentum distribution. Since all the spin and isospin projections are not available for the two-body momentum and coordinate densities, for  $C_{pp}^{s=0}$  we fit the total  $pp$  distribution assuming that the dominant contribution comes from spin=0 (S-wave) pairs. Furthermore, for  $C_{pn}^{s=1}$  ( $C_{pn}^{s=0}$ ) we fit to the  $T=0$  ( $T=1$ )  $pn$  distributions assuming that the dominant contribution comes from spin=1 (spin=0) pairs with the relevant angular momentum. The ratios were extracted independently for both coordinate and momentum space by fitting the two-nucleon density ratios at short distance or high momentum, respectively<sup>3</sup>.

The uncertainties shown include contributions from sensitivity to the fit range, the effect of different two-body correlations<sup>20</sup>, the structure of the three-body contact interaction (for N<sup>3</sup>LO potentials), and the difference between different QMC techniques, conservatively fixed at 10% ( $1\sigma$ ). See Extended Data Fig. 9 and the Supplementary Information for details.

**N<sup>3</sup>LO high-momentum scaling.** The nuclear contact extraction was done systematically in the region  $2.5 \lesssim q \lesssim 4.5 \text{ fm}^{-1}$  for all NN channels and potentials, as described above. Extended Data Fig. 10 shows the two-nucleon relative-momentum distribution ratios,  $n_{NN}(q)/|\varphi_{NN}(q)|^2$ , in <sup>4</sup>He for spin-1  $pn$  and spin-0  $pp$  channels and different interactions. To resolve possible higher-momentum effects, additional statistics were used to compute the two-body momentum distributions shown in the figure. Discontinuities in the ratios are due to nodes in the corresponding universal functions (Extended Data Fig. 2). For the AV4'+UIX, and NV2+3-1a\* interactions, plateaus are clearly identifiable in both the spin-1  $pn$  and spin-0  $pp$  channels, and they consistently extend to

very high momentum. For N<sup>3</sup>LO interactions, in the spin-1  $pn$  channel more complex structures appear, but the contact values extracted at lower momentum remain consistent within uncertainties. In the spin-0  $pp$  channel, instead, a clear high-momentum scaling is difficult to identify, leading to the apparent spin-0  $pp$ - $k$  discrepancy for N<sup>3</sup>LO interactions. This artefact is most likely related to regulator and three-body artefacts, and induced by the occurrence of multiple nearby nodes in the corresponding universal functions. The coordinate-space regulator employed in the NV2+3-1a\* interaction has a Gaussian form<sup>34</sup>, which transforms in a Gaussian regulator in momentum space. The N<sup>3</sup>LO interactions use a different local regulator<sup>32</sup>, which does not keep the same functional form when transformed to momentum space and can induce wiggles at high momentum. When the universal function has a quick drop, like in such a wiggle or in a node, the contribution of two-body SRCs is suddenly decreased, and other contributions become non negligible, complicating the overall picture and its interpretation.

## Data availability

Source data are provided with this paper. All other data that support the plots within this paper and other findings of this study are available from the corresponding author upon reasonable request.

## References

31. Wiringa, R. B. & Pieper, S. C. Evolution of nuclear spectra with nuclear forces. *Phys. Rev. Lett.* **89**, 182501 (2002).
32. Gezerlis, A. et al. Local chiral effective field theory interactions and quantum Monte Carlo applications. *Phys. Rev. C* **90**, 054323 (2014).
33. Lynn, J. E. et al. Chiral three-nucleon interactions in light nuclei, neutron- $\alpha$  scattering, and neutron matter. *Phys. Rev. Lett.* **116**, 062501 (2016).
34. Piarulli, M. et al. Local chiral potentials with  $\Delta$ -intermediate states and the structure of light nuclei. *Phys. Rev. C* **94**, 054007 (2016).
35. Piarulli, M. et al. Light-nuclei spectra from chiral dynamics. *Phys. Rev. Lett.* **120**, 052503 (2018).
36. Baroni, A. et al. Local chiral interactions, the tritium Gamow-Teller matrix element, and the three-nucleon contact term. *Phys. Rev. C* **98**, 044003 (2018).
37. Cruz-Torres, R. et al. Short range correlations and the isospin dependence of nuclear correlation functions. *Phys. Lett. B* **785**, 304–308 (2018).

## Acknowledgements

We thank J. E. Lynn for providing some of the deuteron momentum distributions. We also thank J. Carlson, C. Ciolfi degli Atti, W. Cosyn, S. Gandolfi, A. Lovato, G. A. Miller, J. Ryckebusch, M. Sargsian and M. Strikman for discussions. This work was supported by the US Department of Energy, Office of Science, Office of Nuclear Physics under award nos. DE-FG02-94ER40818, DE-FG02-96ER-40960, DE-AC02-06CH11357, DE-AC05-06OR23177 and DE-SC0013617 (FRIB Theory Alliance Award), the Pazy foundation, and the Israeli Science Foundation (Israel) under grant nos. 136/12 and 1334/16, the NUCLEI SciDAC program, the INCITE program and the Clore Foundation. Computational resources have been provided by the Los Alamos National Laboratory Institutional Computing Program, which is supported by the US Department of Energy National Nuclear Security Administration under contract no. 89233218CNA000001, by the Argonne Leadership Computing Facility at Argonne National Laboratory, which is supported by the US Department of Energy, Office of Science, under contract no. DE-AC02-06CH11357, and by the National Energy Research Scientific Computing Center (NERSC), which is supported by the US Department of Energy, Office of Science, under contract no. DE-AC02-05CH11231.

## Author contributions

D.L., M.P. and R.B.W. performed the many-body QMC calculations. N.B. and R.W. calculated the two-body universal functions. R.C.-T and R.W. analysed the QMC calculated densities and extracted the nuclear contacts. N.B., D.W.H., E.P., A.S., L.B.W. and O.H. initiated and guided the work. All authors contributed to writing the paper and reviewing the results.

## Competing interests

The authors declare no competing interests.

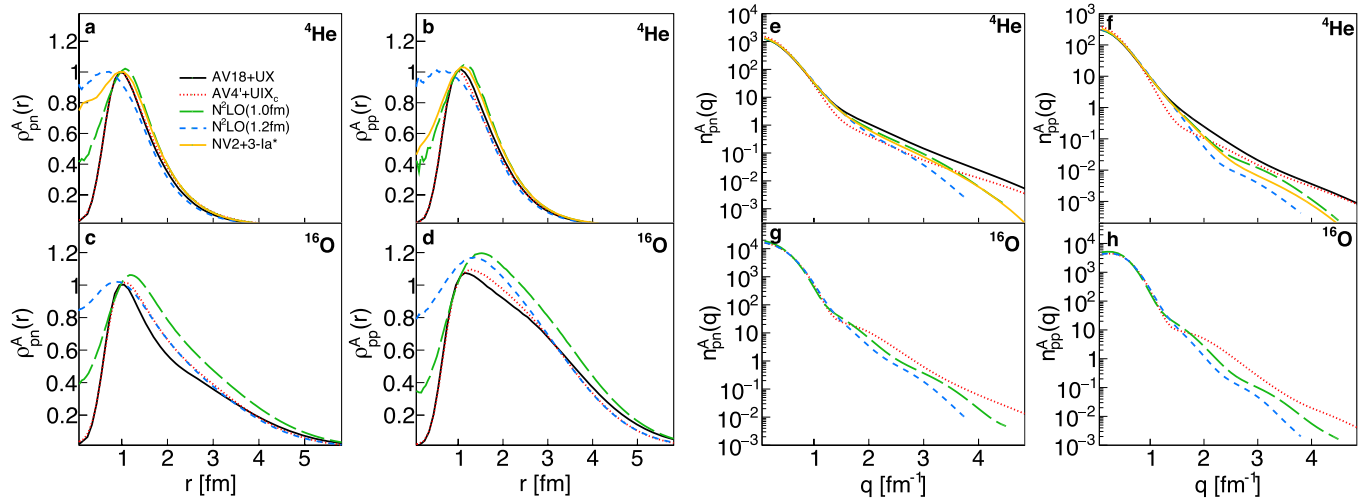
## Additional information

**Extended data** is available for this paper at <https://doi.org/10.1038/s41567-020-01053-7>.

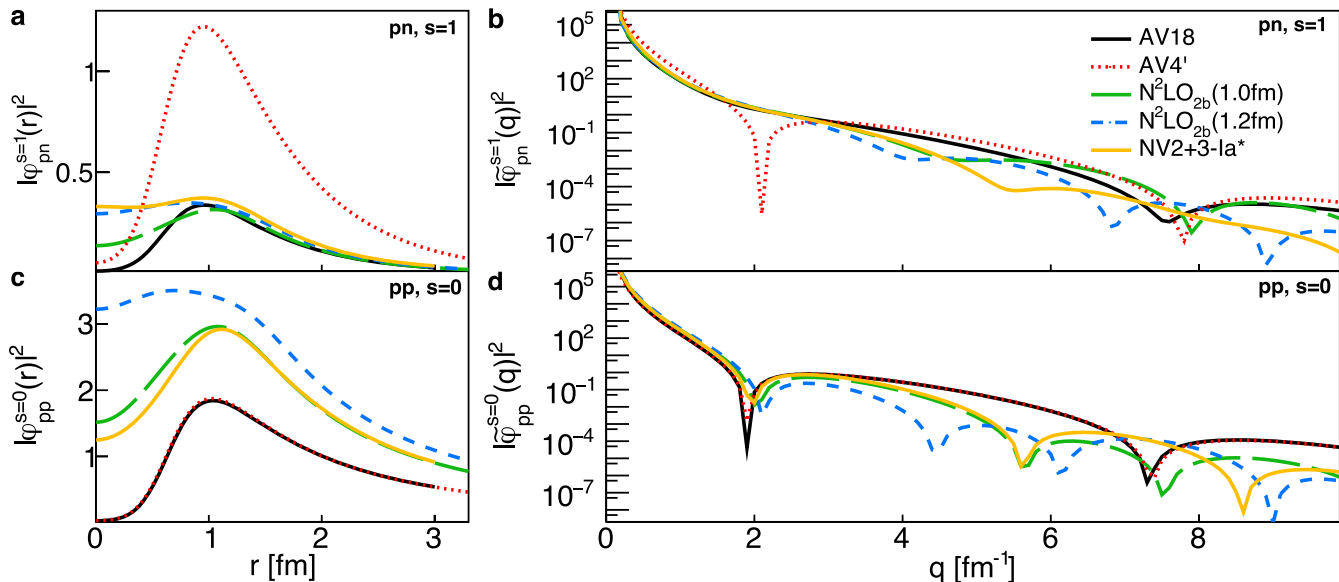
**Supplementary information** is available for this paper at <https://doi.org/10.1038/s41567-020-01053-7>.

**Correspondence and requests for materials** should be addressed to O.H.

**Reprints and permissions information** is available at [www.nature.com/reprints](http://www.nature.com/reprints).



**Extended Data Fig. 1 | Scale and scheme dependence of two-nucleon densities.** Two-nucleon  $\rho_p N^A(r)$  coordinate (**a-d**) and  $(n_p N^A(q)$ ) momentum (**e-h**) space distributions calculated for different nuclei using phenomenological (AV18+UX and AV4'+UIX<sub>c</sub>) and chiral (N<sup>2</sup>LO(1.0fm), N<sup>2</sup>LO(1.2fm), and NV2+3-la\*) potentials. The top (**a, b, e, f**) and bottom (**c, d, g, h**) rows show distributions for  $^4\text{He}$  and  $^{16}\text{O}$  respectively.

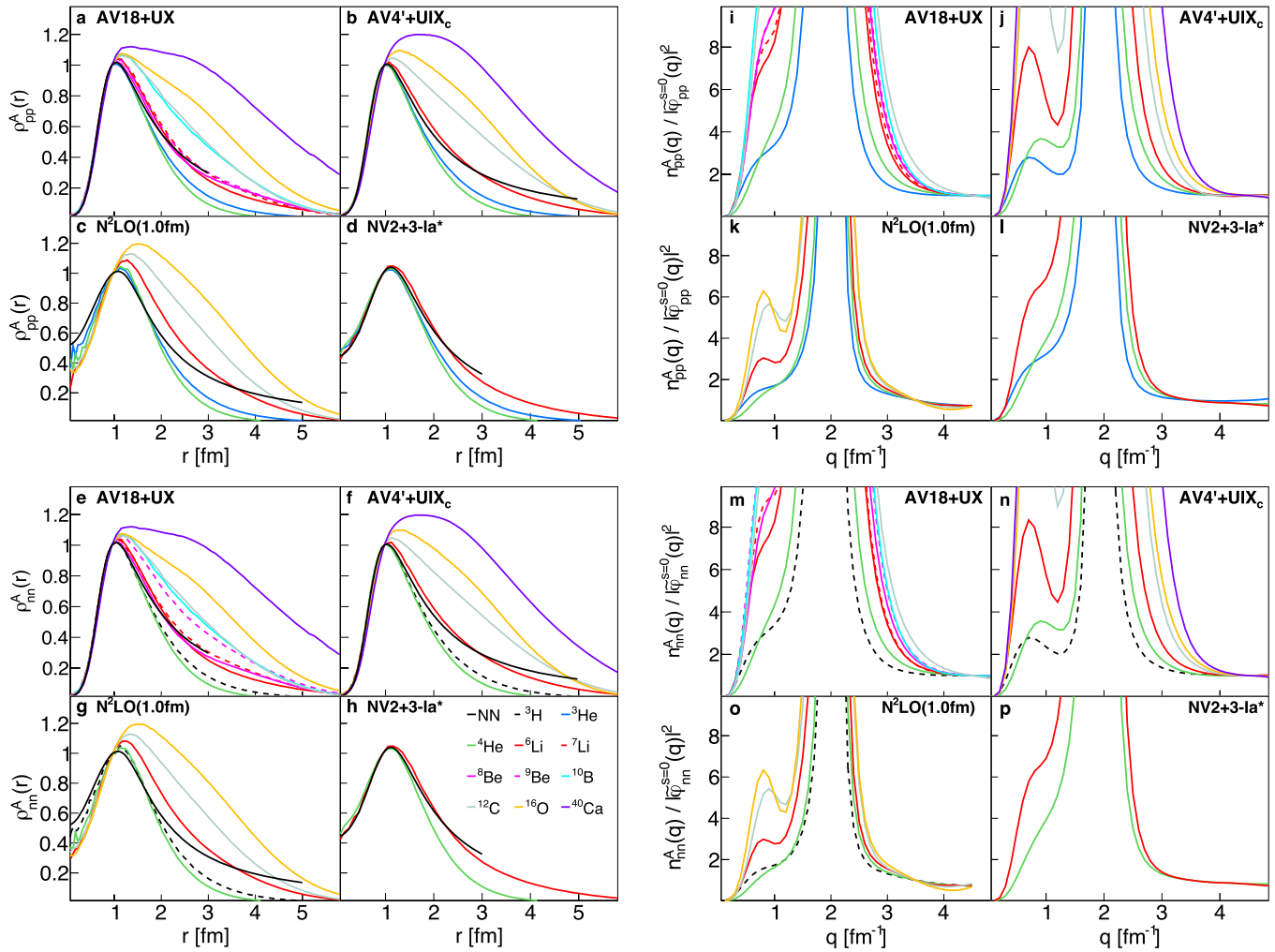


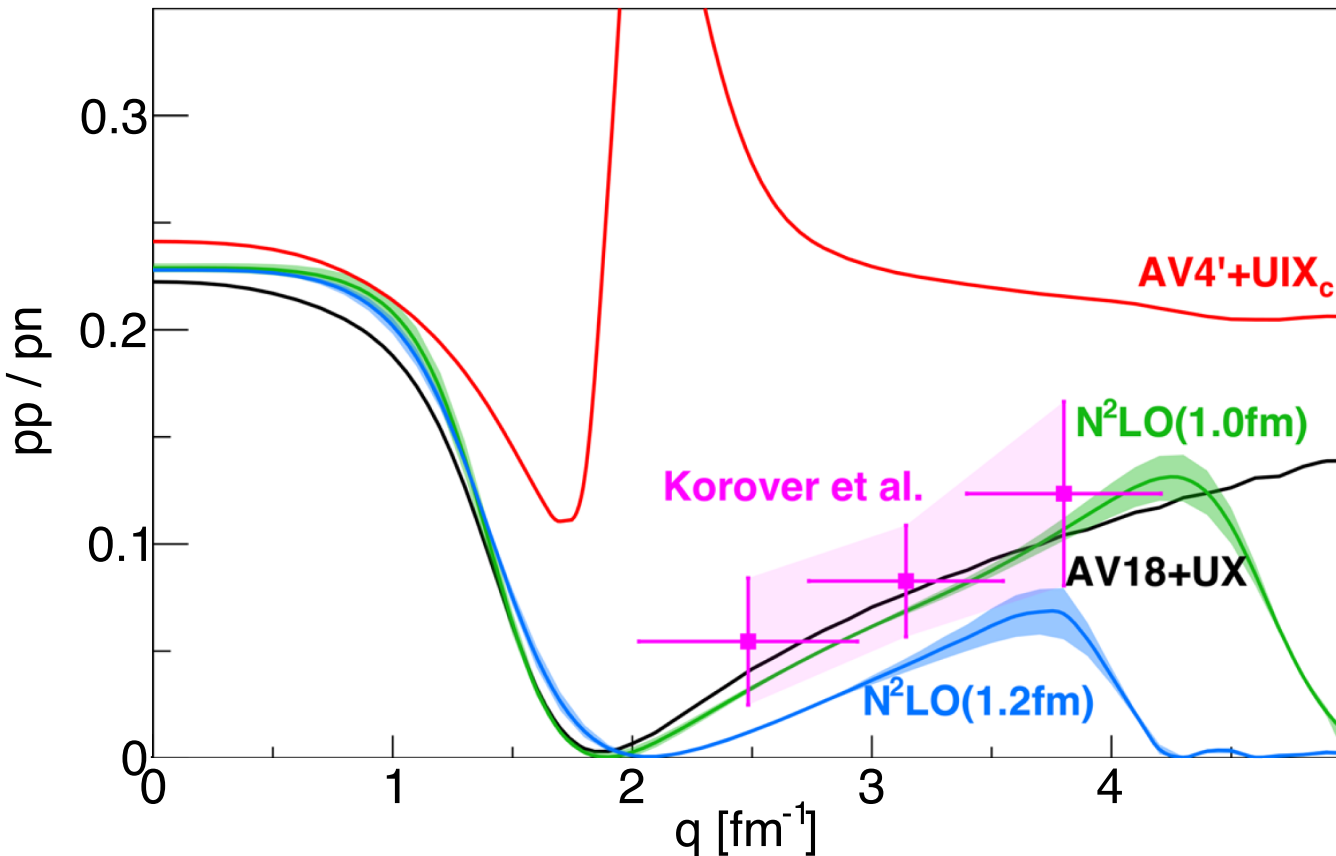
**Extended Data Fig. 2 | Universal two-body functions.** NN interaction model dependence of the universal two-body functions  $|\varphi_N N^\mu|^2$  for spin-1 pn (**a, b**) and spin-0 pp (**c, d**) pairs calculated in both coordinate (**a, c**) and momentum (**b, d**) space. Distributions are shown for both phenomenological (AV18+UX and AV4'+UIX<sub>c</sub>) and chiral ( $N^2LO(1.0\text{fm})$ ,  $N^2LO(1.2\text{fm})$ , and NV2+3- $\text{la}^*$ ) interaction models.

Nucleus	AV18+UX [16, 25, 40]	AV4'+UIX <sub>c</sub> [23, 33]	N <sup>2</sup> LO(1.0fm) [22, 34, 35]	N <sup>2</sup> LO(1.2fm) [22, 34, 35]	NV2+3-Ia* [36, 37]
<i>d</i>	✓	✓	✓	✓	✓
<sup>3</sup> H	✓	✓	✓	✓	—
<sup>3</sup> He	✓	✓	✓	✓	✓
<sup>4</sup> He	✓	✓	✓	✓	✓
<sup>6</sup> Li	✓	✓	✓	✓	✓
<sup>12</sup> C	✓	✓	✓	—	—
<sup>16</sup> O	✓*	✓	✓	—	—
<sup>40</sup> Ca	✓*	✓	—	—	—

\* calculation only available for coordinate-space distributions.

**Extended Data Fig. 3 | Nuclei and models included in this study.** QMC-calculated two-nucleon distributions for different nuclei and NN+3N potentials. Checkmarks indicate calculations used in the current study. All calculations are available for both coordinate and momentum space, except for <sup>16</sup>O and <sup>40</sup>Ca with AV18 (labeled with an \* below), for which the UIX potential is used and results are only available in coordinate space<sup>5</sup>. Calculations with the N<sup>2</sup>LO(1.2fm) potential for heavier systems are not considered in this work due to the large regulator artifacts found for A ≥ 12 (see ref. <sup>20</sup>).

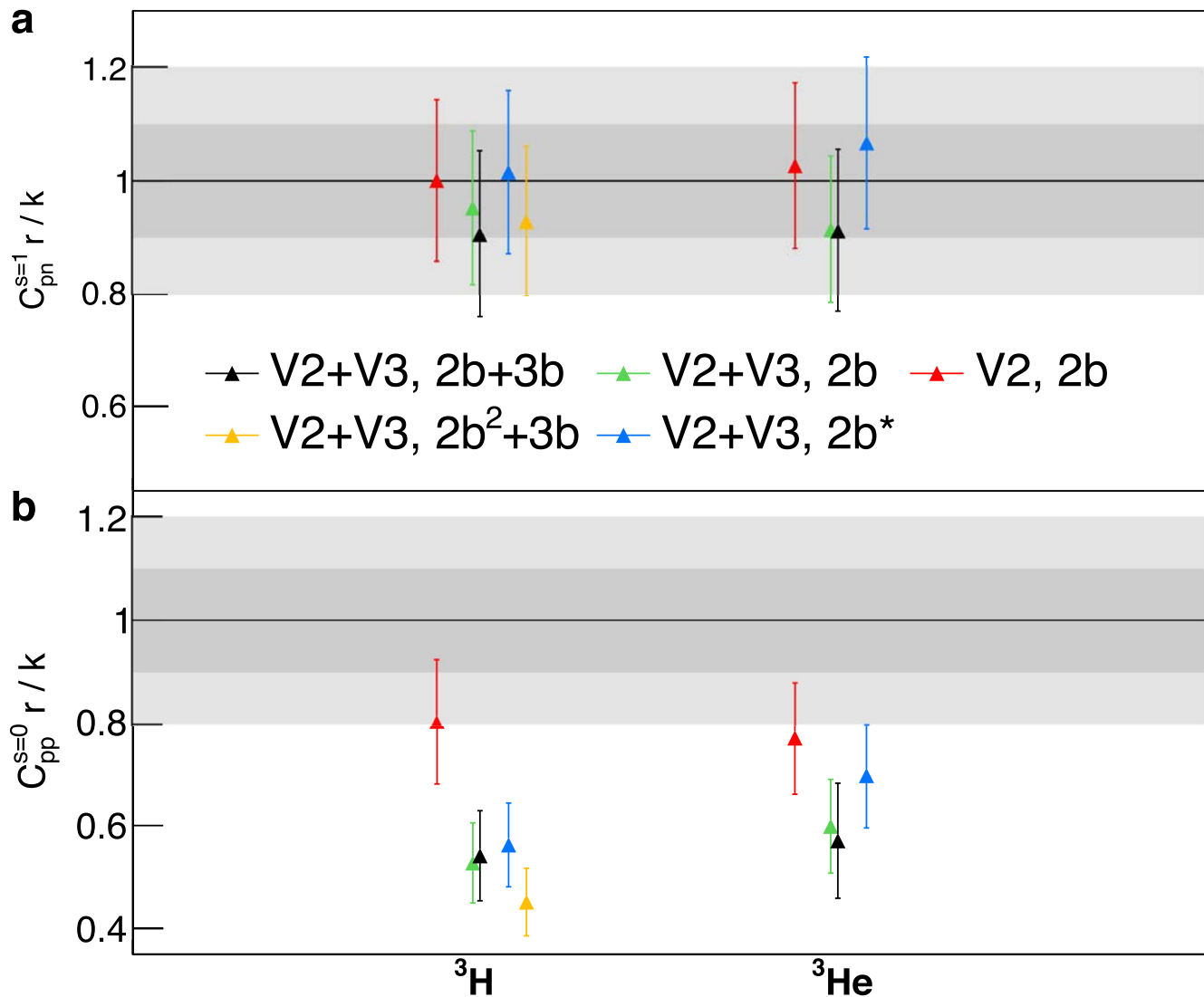




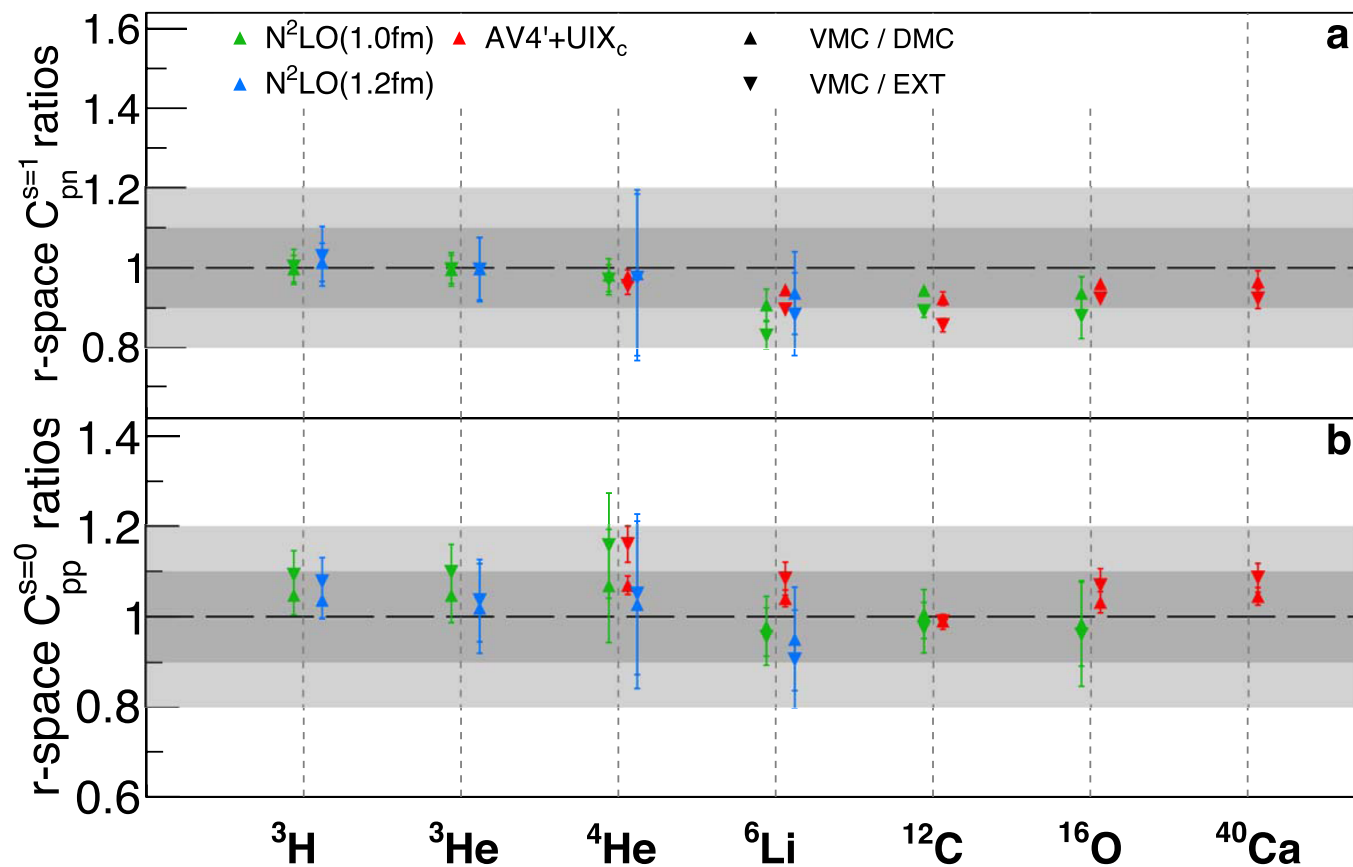
**Extended Data Fig. 5 | pp-to-pn pairs ratio from experiment and theory.** Ratio of pp-to-pn back-to-back pairs in  ${}^4\text{He}$  as a function of pair relative momentum  $q$ ,  $n_p p(Q = 0, q)/n_p n(Q = 0, q)$ , for different NN+3N potentials, compared with the experimental extractions of ref.<sup>8</sup> using (e,e'pp) and (e,e'pn) data. Data error bars show the combined statistical and systematical uncertainties at the 1s or 68% confidence level.

		$C_{pn}^{s=1}$		$C_{pp}^{s=0}$		$C_{pn}^{s=0}$	
		$r$	$k$	$r$	$k$	$r$	$k$
$d$	AV18	4.898 $\pm$ 0.080	4.764 $\pm$ 0.007				
	AV4'	1.186 $\pm$ 0.034	1.165 $\pm$ 0.037				
	N <sup>2</sup> LO(1.0)	4.664 $\pm$ 0.009	4.691 $\pm$ 0.030				
	N <sup>2</sup> LO(1.2)	4.141 $\pm$ 0.010	4.244 $\pm$ 0.032				
	NV2+3-Ia*	3.878 $\pm$ 0.390	3.840 $\pm$ 0.398				
${}^3\text{H}$	AV18	6.246 $\pm$ 0.856	6.441 $\pm$ 0.645	0.549 $\pm$ 0.055	0.590 $\pm$ 0.060	0.295 $\pm$ 0.119	0.311 $\pm$ 0.033
	AV4'	1.533 $\pm$ 0.154	1.515 $\pm$ 0.152	0.544 $\pm$ 0.055	0.532 $\pm$ 0.054	0.270 $\pm$ 0.027	0.281 $\pm$ 0.029
	N <sup>2</sup> LO(1.0)	6.237 $\pm$ 0.718	6.885 $\pm$ 0.789	0.282 $\pm$ 0.032	0.521 $\pm$ 0.060	0.140 $\pm$ 0.015	0.255 $\pm$ 0.063
	N <sup>2</sup> LO(1.2)	5.980 $\pm$ 0.695	6.111 $\pm$ 1.011	0.277 $\pm$ 0.033	0.687 $\pm$ 0.119	0.139 $\pm$ 0.017	0.337 $\pm$ 0.061
${}^3\text{He}$	AV18	6.851 $\pm$ 0.822	6.249 $\pm$ 0.625	0.536 $\pm$ 0.054	0.570 $\pm$ 0.058	0.161 $\pm$ 0.092	0.325 $\pm$ 0.034
	AV4'	1.527 $\pm$ 0.153	1.466 $\pm$ 0.147	0.515 $\pm$ 0.052	0.515 $\pm$ 0.052	0.265 $\pm$ 0.027	0.264 $\pm$ 0.028
	N <sup>2</sup> LO(1.0)	6.113 $\pm$ 0.719	6.703 $\pm$ 0.702	0.259 $\pm$ 0.032	0.454 $\pm$ 0.069	0.135 $\pm$ 0.016	0.264 $\pm$ 0.047
	N <sup>2</sup> LO(1.2)	5.705 $\pm$ 0.870	5.717 $\pm$ 0.730	0.239 $\pm$ 0.041	0.547 $\pm$ 0.079	0.127 $\pm$ 0.022	0.307 $\pm$ 0.057
	NV2+3-Ia*	4.637 $\pm$ 0.573	4.885 $\pm$ 0.491	0.310 $\pm$ 0.031	0.336 $\pm$ 0.034	0.234 $\pm$ 0.053	0.233 $\pm$ 0.024
${}^4\text{He}$	AV18	11.605 $\pm$ 1.161	12.274 $\pm$ 1.232	0.567 $\pm$ 0.057	0.655 $\pm$ 0.071	0.567 $\pm$ 0.057	0.687 $\pm$ 0.075
	AV4'	2.685 $\pm$ 0.272	2.995 $\pm$ 0.300	0.564 $\pm$ 0.057	0.542 $\pm$ 0.055	0.578 $\pm$ 0.059	0.564 $\pm$ 0.057
	N <sup>2</sup> LO(1.0)	10.508 $\pm$ 1.308	12.372 $\pm$ 1.372	0.243 $\pm$ 0.040	0.655 $\pm$ 0.093	0.253 $\pm$ 0.043	0.703 $\pm$ 0.096
	N <sup>2</sup> LO(1.2)	11.111 $\pm$ 2.595	10.446 $\pm$ 2.223	0.263 $\pm$ 0.059	0.851 $\pm$ 0.102	0.281 $\pm$ 0.062	0.934 $\pm$ 0.133
	NV2+3-Ia*	9.200 $\pm$ 0.928	10.143 $\pm$ 1.022	0.333 $\pm$ 0.034	0.355 $\pm$ 0.039	0.333 $\pm$ 0.034	0.504 $\pm$ 0.059
${}^6\text{Li}$	AV18	10.140 $\pm$ 1.015	10.492 $\pm$ 1.056	0.415 $\pm$ 0.042	0.485 $\pm$ 0.058	0.415 $\pm$ 0.042	0.529 $\pm$ 0.071
	AV4'	2.248 $\pm$ 0.225	2.205 $\pm$ 0.222	0.380 $\pm$ 0.038	0.380 $\pm$ 0.038	0.387 $\pm$ 0.039	0.369 $\pm$ 0.039
	N <sup>2</sup> LO(1.0)	8.434 $\pm$ 1.026	9.444 $\pm$ 1.141	0.173 $\pm$ 0.020	0.501 $\pm$ 0.074	0.180 $\pm$ 0.021	0.540 $\pm$ 0.086
	N <sup>2</sup> LO(1.2)	9.011 $\pm$ 1.478	8.650 $\pm$ 1.545	0.185 $\pm$ 0.031	0.668 $\pm$ 0.104	0.197 $\pm$ 0.034	0.749 $\pm$ 0.168
	NV2+3-Ia*			0.250 $\pm$ 0.025	0.282 $\pm$ 0.032		
${}^{12}\text{C}$	AV18	13.135 $\pm$ 1.324	15.876 $\pm$ 1.770	0.716 $\pm$ 0.075	1.140 $\pm$ 0.210	0.716 $\pm$ 0.075	1.244 $\pm$ 0.319
	AV4'	2.458 $\pm$ 0.249	2.676 $\pm$ 0.272	0.547 $\pm$ 0.055	0.653 $\pm$ 0.067	0.559 $\pm$ 0.056	0.558 $\pm$ 0.069
	N <sup>2</sup> LO(1.0)	10.434 $\pm$ 1.044	10.643 $\pm$ 1.094	0.308 $\pm$ 0.033	0.870 $\pm$ 0.095	0.318 $\pm$ 0.034	0.988 $\pm$ 0.161
${}^{16}\text{O}$	AV18	11.372 $\pm$ 1.158		0.676 $\pm$ 0.072		0.676 $\pm$ 0.072	
	AV4'	2.910 $\pm$ 0.293	2.911 $\pm$ 0.307	0.658 $\pm$ 0.066	0.784 $\pm$ 0.084	0.675 $\pm$ 0.068	0.702 $\pm$ 0.086
	N <sup>2</sup> LO(1.0)	9.103 $\pm$ 1.020	10.338 $\pm$ 1.310	0.270 $\pm$ 0.034	0.781 $\pm$ 0.173	0.275 $\pm$ 0.033	0.928 $\pm$ 0.365
${}^{40}\text{Ca}$	AV18	11.570 $\pm$ 1.196		0.723 $\pm$ 0.081		0.723 $\pm$ 0.081	
	AV4'	3.284 $\pm$ 0.339	4.476 $\pm$ 0.460	0.834 $\pm$ 0.084	1.329 $\pm$ 0.144	0.854 $\pm$ 0.086	1.357 $\pm$ 0.164

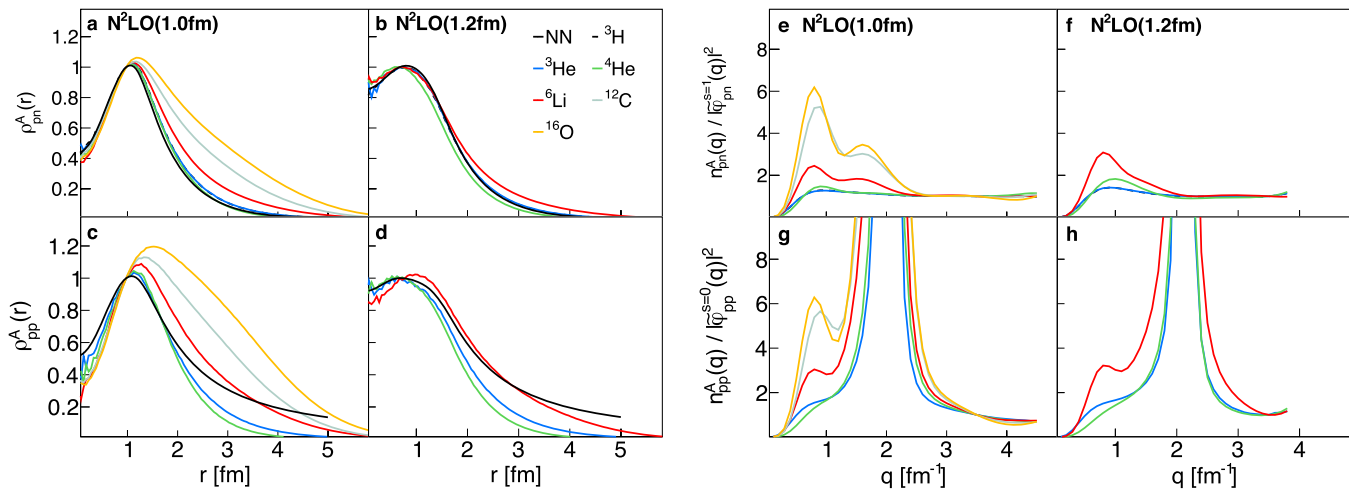
**Extended Data Fig. 6 | Nuclear contacts values.** The extracted contact values have been divided by  $A/2$  and multiplied by 100 to give the percent of nucleons above  $k_F$ . For symmetric nuclei,  $C_n n^{s=0} = C_p p^{s=0}$ . In the case of  ${}^3\text{He}$ ,  $C_n n^{s=0}$ , as there is only one neutron in this nucleus. In the case of  ${}^3\text{H}$ ,  $C_p p^{s=0}$ , as there is only one proton in this nucleus, and the values shown under  $C_p p^{s=0}$  correspond to  $C_n n^{s=0}$ .



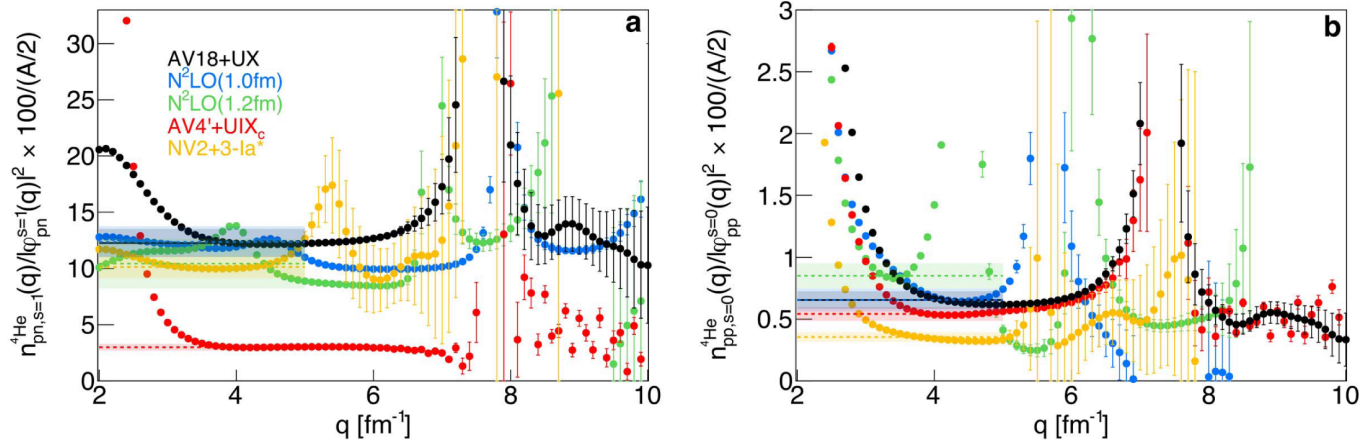
**Extended Data Fig. 7 | Impact of three body forces and correlations on N<sup>2</sup>LO k-r consistency.** Ratios of coordinate-space to momentum-space pn (**a**) and pp (**b**) contact terms in  ${}^3\text{H}$  and  ${}^3\text{He}$  for the N<sup>2</sup>LO(1.0fm) interaction. The contact values for  ${}^3\text{H}$  in the spin-0 pp panel corresponds to the spin-0 nn values, as there are no pp pairs in this nucleus. V2+V3 refers to calculations employing the full 2+3-body Hamiltonian, while results labelled as V2 are obtained turning off the 3-body potential. The second part of the labels refers instead to different wave functions, obtained by optimizing different correlations for the given V2+V3 or V2 Hamiltonian: 2b+3b for the full 2+3-body correlations; 2b<sup>2</sup>+3b for the full 2+3-body correlations, where more sophisticated 2b correlations are used (see ref. <sup>20</sup>); 2b for 2-body correlations only; 2b\* for 2-body correlations only, obtained by turning off the 3-body correlations of the 2b+3b wave function (no re-optimization).



**Extended Data Fig. 8 | Calculation accuracy estimation.** Ratios of contacts extracted from VMC densities to contacts extracted from DMC and extrapolated (EXT = 2 × DMC - VMC<sup>20</sup>) distributions for pn (a) and pp (b) contacts. Error bars show the combined statistical and extraction systematical uncertainties at the 1 $\sigma$  or 68% confidence level.



**Extended Data Fig. 9 | Scale dependence of N<sup>2</sup>LO-based QMC calculations.** **a-d**, Relative-distance densities for pn (**a**, **b**) and pp (**c**, **d**) pairs for several nuclei (colored lines) integrated over R and compared with the two-body universal functions (black lines). For each interaction, all calculations are scaled to have the same value at  $\sim 1$  fm and show the same short-distance behavior for all nuclei. **e-h**, same as the left panel but for the two-nucleon momentum-space distribution ratios,  $n_p n^A(q) / |\tilde{\varphi}_p \eta^{s=1}(q)|^2$  (**e**, **f**) and  $n_p n^A(q) / |\tilde{\varphi}_p p^{s=0}(q)|^2$  (**g**, **h**) normalized to unity at  $q = 3.5$  fm $^{-1}$ . Scaling is clearly observed at high momenta. The N<sup>2</sup>LO 1.0fm and 1.2fm distributions are only shown up to 4.4 and 3.8 fm $^{-1}$  respectively, above which statistics is poor and regulator/cutoff artifacts dominate.



**Extended Data Fig. 10 |  ${}^4\text{He}$  two-nucleon relative-momentum distribution ratios,  $n_N N(q)/|\tilde{\varphi}_N N(q)|^2$ .** Spin-1 pn (**a**) and spin-0 pp (**b**) distributions. All curves are divided by  $A/2 = 2$  and multiplied by 100. Results for five potentials are shown: AV18+UX, AV4'+UIX<sub>c</sub>, NV2+3-la\*, N<sup>2</sup>LO  $R_0 = 1.0\text{ fm}$ , and N<sup>2</sup>LO  $R^0 = 1.2\text{ fm}$ . Horizontal lines with error bands correspond to the extracted contacts (see Methods and Extended Data Fig. 6). For N<sup>2</sup>LO potentials, results for one choice of three-body contact operators is shown here. Error bars show the monte-carlo statistical uncertainties of the QMC calculation at the 1s or 68% confidence level.